The abundance and isotopic composition of water in eucrites

T. J. Barrett, J. J. Barnes, R. Tartèse, M. Anand, I. A. Franchi, R. C. Greenwood, B. L. A. Charlier, M. M. Grady

The Meteoritical Society

Meteoritics & Planetary Science 1–15 (2016)
doi: 10.1111/maps.12649

The abundance and isotopic composition of water in eucrites

T. J. BARRETT[1*], J. J. BARNES[1], R. TARTÈSE[1,2], M. ANAND[1,3], I. A. FRANCHI[1], R. C. GREENWOOD[1], B. L. A. CHARLIER[1], and M. M. GRADY[1,3]

[1]Planetary and Space Sciences, The Open University, Milton Keynes MK7 6AA, UK
[2]Institut de Minéralogie, de Physique des Matériaux et de Cosmochimie, Muséum National d'Histoire Naturelle, Sorbonne Universités, CNRS, UPMC & IRD, 75005 Paris, France
[3]Department of Earth Sciences, Natural History Museum, London SW75BD, UK
[*]Corresponding author. E-mail: thomas.barrett@open.ac.uk

(Received 14 October 2015; revision accepted 04 March 2016)

Abstract–Volatile elements play a key role in the dynamics of planetary evolution. Extensive work has been carried out to determine the abundance, distribution, and source(s) of volatiles in planetary bodies such as the Earth, Moon, and Mars. A recent study showed that the water in apatite from eucrites has similar hydrogen isotopic compositions compared to water in terrestrial rocks and carbonaceous chondrites, suggesting that water accreted very early in the inner solar system given the ancient crystallization ages (~4.5 Ga) of eucrites. Here, the measurements of water (reported as equivalent H_2O abundances) and the hydrogen isotopic composition (δD) of apatite from five basaltic eucrites and one cumulate eucrite are reported. Apatite H_2O abundances range from ~30 to ~3500 ppm and are associated with a weighted average δD value of $-34 \pm 67‰$. No systematic variations or correlations are observed in H_2O abundance or δD value with eucrite geochemical trend or metamorphic grade. These results extend the range of previously published hydrogen isotope data for eucrites and confirm the striking homogeneity in the H-isotopic composition of water in eucrites, which is consistent with a common source for water in the inner solar system.

INTRODUCTION

Asteroids formed early within the solar nebula (~10^5–10^7 years after CAIs; Chambers and Wetherill 2001; O'Brien et al. 2014) and are likely to have retained information regarding the very earliest processes occurring in the proto-planetary disk. They are, therefore, crucial for understanding how the solar system formed and evolved. Furthermore, because of their antiquity, composition, and heliocentric distance, asteroids may also provide clues to the delivery of water and other volatiles to the early Earth, the Moon, and more generally to the inner solar system, which is of prime importance in the context of development of habitable environments on the early Earth.

The howardite–eucrite–diogenite (HED) meteorites are a group of basaltic achondrites derived from a common parent body believed to be the asteroid 4 Vesta (McCord et al. 1970; Consolmagno and Drake 1977; Binzel and Xu 1993). The HED meteorites comprise the largest suite of crustal rocks available from a differentiated asteroid, and account for 3% of all meteorites collected globally, ~5% of all falls, and ~70% of all achondrites (Meteoritical Bulletin http://www.lpi.usra.edu/meteor/metbull.php; Janots et al. 2012). Since HED meteorites are some of the oldest achondrites, typically with crystallization ages from 4547 to 4559 Ma (Misawa et al. 2005; Zhou et al. 2013), determining their water inventory may provide crucial insights into the processes involved in the early water delivery to the inner solar system.

The volatile inventories of volatile-depleted bodies such as the Moon or Vesta have been poorly constrained until recently because of the limitations in analytical techniques. However, recent analytical advances in secondary ion mass spectrometry (SIMS) techniques have permitted the successful in situ detection of H in volcanic glasses and minerals such as

apatite from a variety of lunar and eucrite samples (Saal et al. 2008; Greenwood et al. 2011; Hauri et al. 2011; Barnes et al. 2013; Tartèse et al. 2013; Sarafian et al. 2014). Similar to lunar and Martian samples, eucrites contain two major phosphate minerals—apatite and merrillite. Apatite ($Ca_5[PO_4]_3[F, Cl, OH]$) is a widely distributed accessory phase in planetary materials, and has been used as a recorder of the relative abundances of the volatile species OH, F, and Cl in magmas and magmatic source regions (Patiño Douce and Roden 2006; McCubbin et al. 2011, 2014; Patiño Douce et al. 2011; Barnes et al. 2013; Sarafian et al. 2013, 2014; Tartèse et al. 2013, 2014b). In contrast, the phosphate merrillite ($[Mg,Fe]_2REE_2Ca_{16}P_{14}O_{56}$) does not incorporate significant volatiles, but is a major reservoir of rare-earth elements (REEs) (20,000–30,000 times chondrite, compared to apatite at 500–1000 times chondrite for light REEs; Delaney et al. 1984). In this study, we focus on apatite as it is the only known volatile-bearing mineral in eucrites (Delaney et al. 1984; Sarafian et al. 2013). Apatite contains hydrogen in the form of structurally bound OH, but in this contribution the measured OH abundance is converted to its weight equivalent H_2O for the purposes of comparing the data with those in the literature.

Currently the water inventory and isotopic composition of eucrites is poorly understood partly owing to a limited number of studies (Sarafian et al. 2013, 2014). Here, we present a comprehensive data set for the H_2O abundance and H isotopic composition of apatite in a suite of basaltic eucrites, representative of the principal geochemical trends and metamorphic grades, as well as for cumulate eucrites, which have not been analyzed previously. The isotopic signatures of water in eucritic apatite are assessed and processes, such as volatile degassing, which could have affected these signatures, are explored. By combining these new results with published data, the origin of volatiles in the inner solar system and the mechanisms/processes of volatile transport across the solar system are investigated.

CRITERIA FOR SAMPLE SELECTION AND PETROLOGY OF THE STUDIED SAMPLES

Based on their petrographic textures, monomict and unbrecciated eucrites are subdivided into cumulate and noncumulate (basaltic) groups (Stolper 1977; B.V.S.P. 1981; Mayne et al. 2009). The basaltic eucrites can be further subdivided geochemically into the Main Group-Nuevo Laredo and Stannern trends based on their magnesium numbers, Mg# (or their FeO_{total}/MgO weight ratio), Ti content, and incompatible trace element abundances (Stolper 1977; Hsu and Crozaz 1996; Hutchison 2004; Barrat et al. 2007). The Main Group-Nuevo Laredo trend comprises the majority of the eucrites and is widely regarded as representing a fractional crystallization trend, where incompatible element abundances increase with Fe enrichment (Stolper 1977; Warren and Jerde 1987; Mittlefehldt and Lindstrom 2003). The Stannern trend eucrites are very similar to the main group for major elements. However, they contain greater abundances of Ti and incompatible trace elements (Barrat et al. 2000, 2007; Hutchison 2004). Barrat et al. (2007) suggested that contamination of Main Group-Nuevo Laredo trend eucrites by crustal melts can explain both the elevated incompatible element concentrations and the distinctive Eu, Sr, and Be anomalies exhibited by the Stannern trend eucrites when normalized to a representative Main Group eucrite. This crustal partial melt would leave behind a residual melt associated with LREE depletion, which Yamaguchi et al. (2009) observed in several eucrites and assigned them to a potential third geochemical trend.

The samples studied here are broadly representative of eucrites as a whole since they represent each of the five criteria listed below (see Table 1 for more details):

1. Samples were selected to represent the different geochemical trends, the Main Group-Nuevo Laredo trend, Stannern trend, residual, and cumulate eucrite.
2. To ensure both a representative sampling and to enable comparisons with the existing data set, both falls and finds were studied. To reduce the potential influence of terrestrial contamination on measured values, however, eucrite falls were preferred where possible.
3. Eucrites with a variety of metamorphic grades, between type 4 and 6 on the pyroxene thermal scale (Takeda and Graham 1991; Yamaguchi et al. 1996), were selected in order to examine whether a relationship exists between metamorphic grade and volatile composition.
4. A range of breccia types was chosen in order to assess any lithological-volatile patterns.
5. Samples with a range of cosmic ray exposure (CRE) ages were selected.

The amount of water reported by previous studies of apatite in eucrites ranges between ~80 to 7800 ppm H_2O (Sarafian et al. 2013). Sarafian et al. (2014) expanded on their initial study by reporting the *H* isotope composition of the water in five eucrites using the standard δD (per mil, ‰) notation whereby:

$$\delta D = \left\{ \left(\frac{\frac{D}{H}_{\text{sample}}}{\frac{D}{H}_{\text{VSMOW}}} \right) - 1 \right\} * 1000 \quad (1)$$

The reference used is VSMOW with a D/H ratio of 155.76×10^{-6} (Hagemann et al. 1970). The average δD

Table 1. Main characteristics of the meteorites studied. Cosmic ray exposure (CRE) ages for eucrites Stannern and Millbillillie are taken from Miura et al. (1998); Sioux County and Moore County ages are from Eugster and Michel (1995).

Meteorite	Find/fall	Geochemical trend	Brecciation	Weathering grade	Metamorphic grade	CRE age (Ma)
Dar al Gani 844	Find		Polymict	W3	Type 6	
Dar al Gani 945	Find	Residual	Brecciated	W1	Type 4	
Millbillillie	Fall	Main Group	Polymict		Type 6	20.08
Moore County	Fall	Cumulate	Unbrecciated			7.30
Sioux County	Fall	Main Group	Polymict		Type 5	20.60
Stannern	Fall	Stannern Trend	Monomict		Type 4	35.10

value of water measured in apatite from five eucrites was $-162 \pm 127‰$ (2σ) (Sarafian et al. 2014).

Samples

Representative BSE images illustrating the textural and petrological context of the apatite grains analyzed in this study are given in Fig. 1.

Dar al Gani 844

Dar al Gani (DaG) 844 is a highly fractured, polymict breccia composed of large coarse-grained clasts supported in a fine-grained matrix. The lack of Ca zonation in pyroxene and inversion of pigeonite to orthopyroxene suggests that it is a type 6 eucrite (Takeda and Graham 1991). Minor phases include apatite, troilite, ilmenite, chromite, zircon, and merrillite. Apatite occurs as subhedral to anhedral crystals within fine-grained mesostasis areas, typically ranging in length from 5 to 20 μm, and is associated with other late-stage minerals. Apatite and merrillite were found together only in one area of this sample (Fig. 1).

Dar al Gani 945

Dar al Gani (DaG) 945 is a coarse-grained granulitic eucrite mainly composed of subhedral type 4 pyroxene and plagioclase, with some fine-grained relict mesostasis regions. The sample shows well-defined 120° triple junctions indicative of significant recrystallization (Yamaguchi et al. 2009). Minor phases include apatite, zircon, ilmenite, a silica polymorph, and chromite, all of which usually occur within the late-stage mesostasis areas. Apatite grains in this sample are abundant and subhedral, ranging in size from ~10 to 50 μm in the longest dimension (Fig. 1).

Millbillillie

Millbillillie is a polymict breccia comprising type 6 pyroxene; an indicator of significant thermal metamorphism (Takeda and Graham 1991; Yamaguchi et al. 1994, 1996). The sample consists of two dominant rock types. The first lithology displays areas with a fine-grained subophitic, basaltic texture, in which the interstitial pyroxene has recrystallized to a fine-grained granoblastic texture. This first lithology may have formed as a fast-cooling lava, possibly near the surface of the parent body. The second lithology is a coarse-grained granulitic breccia (Bobe et al. 1989; Yamaguchi et al. 1994, 1996). Minor phases occur in both lithologies and include chromite, apatite, ilmenite, a silica polymorph, troilite, merrillite, and zircon. Apatite grains in both lithologies range from ~10 to 100 μm in the longest direction. In the coarse-grained granulitic lithology apatite is typically anhedral. Apatite has also been found within the finer grained lithology. Only apatite grains from the coarser grained (granulitic) region were analyzed in this study (Fig. 1).

Sioux County

Sioux County is a heavily fractured, coarse-grained breccia. Pyroxene crystals are mainly type 5. According to the Meteoritical Bulletin Database, Sioux County is monomict; however, Yamaguchi et al. (1997) suggested that there are also minor amounts of type 4 and type 6 pyroxene within the sample, suggestive of a polymict breccia. Plagioclase occurs as a mixture of large fractured grains (~a few mm), or as fine-grained crystals interstitial to the coarser grains. Minor phases include apatite, troilite, zircon, ilmenite, merrillite, and a silica polymorph. Apatite grains are mainly subhedral, ranging in size from 10 to 60 μm, occurring interstitially between the larger silicate minerals (Fig. 1).

Stannern

Stannern is a type 4 monomict breccia displaying medium-grained subophitic texture. Late-stage fine-grained mesostasis pockets typically occur interstitially between the large (several mm in the longest axis) plagioclase laths. Minor phases include apatite, ilmenite, troilite, a silica polymorph, merrillite, and zircon.

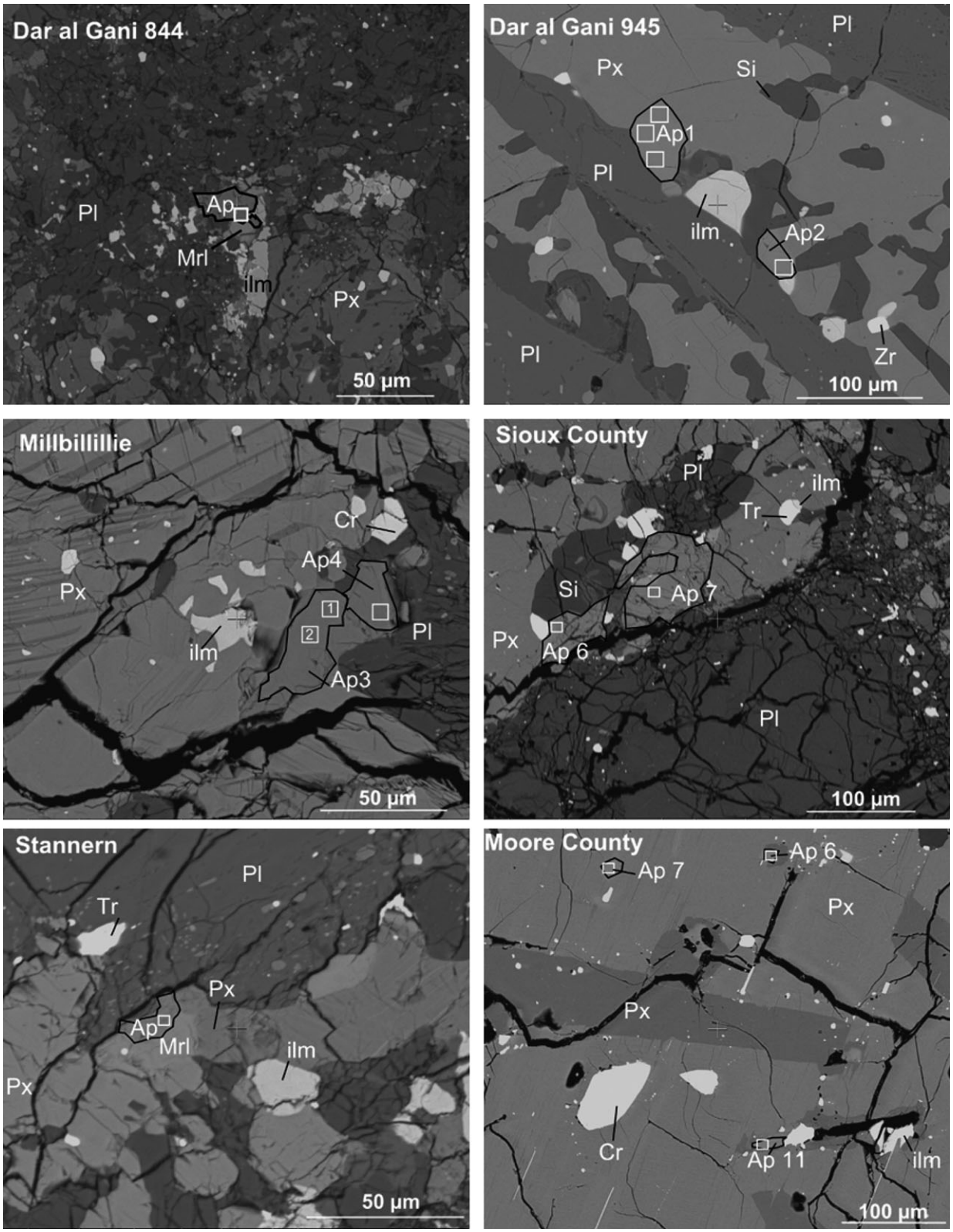

Fig. 1. Representative backscatter electron (BSE) images of each of the eucrite samples. Pl = plagioclase, Px = pyroxene, Ap = apatite, Mrl = merrillite, ilm = ilmenite, Cr = chromite, Tr = troilite, Si = silica phase, Zr = zircon. Solid white squares represent approximate location of SIMS raster area.

Apatite in Stannern occurs as subhedral to anhedral crystals, which range in size from ~10 to 100 μm in length and are associated with relict mesostasis (Fig. 1). In one region of Stannern (discussed later), apatite appears to have cocrystallized with pyroxene, whereas apatite in other areas appears to have crystallized later, along with other late-stage phases such as ilmenite and troilite.

Moore County

Moore County is a coarse-grained, unbrecciated cumulate eucrite. The meteorite consists of large, mm-sized euhedral to subhedral pyroxene grains with coarse augite exsolution features (~15–100 μm) and granular plagioclase. Minor phases include tridymite, ilmenite, chromite, troilite, Fe-Ni metal, and apatite (Hess and Henderson 1949; Mayne et al. 2009). Apatite primarily occurs as subhedral or acicular grains typically 10–50 μm in longest dimension (Fig. 1).

METHODS

Secondary Electron Microscopy

Each polished thin-section was carbon-coated using an EMITECH K950X Turbo carbon sputter coater and examined at The Open University using a Quanta 3-D Focused Ion Beam Scanning Electron Microscope (FIB SEM) fitted with an Oxford Instrument INCA energy dispersive X-ray detector. An electron beam with an acceleration voltage of 20 kV and a beam current of 0.6 nA was used for the acquisition of all the backscattered electron (BSE) images and X-ray maps. The latter were acquired for the entirety of each section to locate phosphates, which could be achieved readily on account of their elevated and concordant Ca and P X-ray counts.

Once located, high-resolution BSE and secondary electron (SE) images of the phosphates were collected. Rapid energy dispersive X-ray spectroscopy (EDS) spot analyses (~30 s exposure) were then acquired to distinguish apatite from merrillite (short exposure at low beam currents does not affect the water contents or δD values of apatite; Barnes et al. 2013). Apatite grains suitable for further analysis were then selected based on their dimensions (>10 μm × 10 μm) and relative lack of fractures and inclusions.

NanoSIMS Protocol

Prior to ion-probe analyses, the carbon coat used for SEM analysis was removed and replaced with a ~30 nm gold coat. Samples were stored in a vacuum oven at ~55 °C for at least 24 h. Once in the airlock, the sample was left to degas under vacuum at ~55 °C for at least a day before transferring it to the vessel chamber. Analyses were conducted using a Cameca NanoSIMS 50L at the Open University following a well-established protocol (Barnes et al. 2013, 2014; Tartèse et al. 2013). Prior to analysis, areas (typically 12 μm × 12 μm) containing target apatite grains were presputtered to remove surface contamination, using a large Cs^+ primary beam of ~600 pA current with an acceleration voltage of 8 kV, the sample surface being at −8 kV. The instrument was set up in multicollection mode, measuring negative secondary ions of ^1H, D, ^{12}C, and ^{18}O on electron multipliers with a mass resolving power of ~4300 (Cameca definition) sufficient to resolve $^1H_2^-$ from D^-. An electron flood gun was used to compensate for charge build up. For analysis, the beam current was lowered to ~250 pA and the raster area was reduced to a 10 μm × 10 μm area, with a 25% electronic gating set in order to collect only secondary ions emitted from the central zone (5 μm × 5 μm) of the analysis area. Secondary ion images of ^1H and ^{12}C were monitored in real time during presputtering to ensure that the area to be analyzed was free of cracks or hotspots indicative of contamination. Monitoring the ^1H and ^{12}C ion beam intensities during analyses allowed the identification of cracks originally hidden beneath the surface. In such cases, only portions of the secondary ion signals corresponding to analysis of pristine material were considered and isolated using the NanoSIMS DataEditor software (Frank Gyngard, Washington University). In cases where apatite grains showed extensive cracks or were particularly small, the raster size was reduced to as small as 4 μm × 4 μm. The D/H and $^1H/^{18}O$ ratio of standards analyzed at smaller raster sizes are comparable to those obtained during typical standard measurements. Analysis rasters were divided into 64 × 64 pixels and the counting time was set to 132 μs/pixel, corresponding to 0.54 s/cycle. Each analysis consisted of 2000 cycles, corresponding to a total analysis time of about 18 min. Typical counts per second of H and D were 9.3×10^3 and 1.9, respectively, for samples with ~1000 ppm H_2O and 8.5×10^2 and 1.9×10^{-1}, respectively, for ~100 ppm H_2O samples. Terrestrial apatite standards (Ap004, Ap005, Ap018, Ap020 see McCubbin et al. 2012), along with a nominally anhydrous San Carlos olivine, were used to correct for instrumental mass fractionation of H isotopes and to calculate both apatite water contents and the total background water contribution.

Background water in the instrument can have a large effect on the D/H ratio measured in apatite, especially when apatite has a very low H_2O content. The raw data for measured water contents in apatite

were first corrected for the background contribution, which ranged from the equivalent of 14–31 ppm H_2O depending on the analytical session. The background was determined using the $^{1}H/^{18}O$ ratios measured on the nominally anhydrous San Carlos olivine and the calibration slope for the corresponding analytical session. The background water content measured on San Carlos olivine represents the total background comprising detector dark noise (measured to be 0.0016 cps across all detectors), hydrogen desorbed by the electron beam, and the contribution from other sources (e.g., epoxy degassing). The raw D/H ratios were corrected based on the percentage contribution of the instrument background to the measured H_2O content, and the δD value of the instrument background (132 ± 150‰, based on 44 repeated measurements on the nominally anhydrous San Carlos olivine), following the relationship:

$$D/H_{\text{measured}} = (f \times D/H_{\text{apatite}}) + ((1 - f) \times D/H_{\text{background}}) \quad (2)$$

where f is the proportion of H emitted from the apatite and $1 - f$ the proportion of H attributed to the instrument background. The raw data along with background corrected data are listed in Table 2.

Spallation Correction

Spallation is a process caused by the interaction of cosmic rays with a rock residing within a few meters of the surface of a planetary body, which causes an increase in δD values through the spallogenic production of D. Effects of this process on δD values can be corrected by using the cosmic ray exposure (CRE) ages of the studied samples and the production rates of spallogenic H and D (e.g., Saal et al. 2008; Barnes et al. 2014). The cosmic ray flux for the asteroid 4-Vesta is not known; however, it is expected to be lower than that for the Moon, since 4-Vesta is at a greater heliocentric distance. Therefore, using the lunar production rates (2×10^{-10} mol H_2 g^{-1} Ma^{-1} for H and 0.5×10^{-12} mol D_2 g^{-1} Ma^{-1} for D; see, Merlivat et al. [1976]; Saal et al. [2013]; Barnes et al. [2014], and references therein) is likely to result in maximum corrections for cosmic ray exposure. Since no CRE age currently exists for DaG 844 and DaG 945, these samples were corrected for the effects of spallation using the oldest grouping of CRE ages for HED meteorites (38 Ma) to give a maximum corrected value. For the studied samples, correction for spallation effects did not change δD values significantly (Table 2) since their CRE ages are relatively young.

RESULTS

H_2O Content and δD Signatures in Apatite

In total, 32 measurements were carried out on 23 apatite grains from six samples, and the results are listed in Table 2 and plotted in Fig. 2. The measured apatite H_2O contents span more than three orders of magnitude, from ~30 ppm in Moore County to 3500 ppm in DaG 844. Apatite in Stannern displays the largest variation in water content, with a bimodal distribution clustering at ~40 ppm and 1600 ppm, the lower values coming from a single grain out of the three grains measured (Fig. 2e). In DaG 945, on the other hand, apatite grains display relatively restricted variations in H_2O content, ranging from 54 ± 2 to 229 ± 7 ppm (Fig. 2b). Apatite in this sample, however, is characterized by the largest variation in H-isotopic composition, with δD values ranging from +697 ± 403‰ to −441 ± 379‰ (Fig. 2b). The large uncertainties associated with the δD values for all samples (DaG 945 in particular) are related to the poor counting statistics associated with the low water contents of some apatite grains, and hence very low total counts of D. The cumulate eucrite Moore County contains apatite grains with the lowest water contents of 26 ± 1 to 124 ± 3 ppm (Fig. 2f). The δD values of the wettest apatites (>800 ppm H_2O) studied in DaG 844, Millbillillie and Stannern are similar and range from −174 ± 185‰ to +84 ± 122‰ (Figs. 2a, 2c, 2e, and 3). In some cases, it was possible to obtain multiple measurements within the same apatite grain (Fig. 2). With the exception of a single grain in Millbillillie it was found for most cases that there is little intragrain variability in H_2O content.

DISCUSSION

Potential Influence of Terrestrial Alteration

Of the six eucrites analyzed, four are falls, which are likely to have suffered minimal terrestrial alteration (Table 1). The remaining two eucrites, DaG 844 and DaG 945, are hot desert finds with weathering grades of W3 and W1, respectively. In these finds it is important to consider the potential terrestrial alteration history when assessing the indigenous D/H signatures of the water within analyzed apatite grains. The H-isotopic composition of central Saharan meteoric water and groundwater has been shown to vary between −70‰ and +20‰ (Saighi et al. 2001), which overlaps with the D/H ratios that were measured in these two samples. Apatite in DaG 945 contains water displaying a range in δD from −441 ± 379‰ (2σ) to

Table 2. Background and spallation corrected δD values, water contents, and the associated uncertainties for apatite in eucrites. Values for f used in Equation 2 are also provided.

Sample ID	δD value raw (‰)	δD value bkg corr (‰)	δD value final (‰)	2σ (‰)	f (%)	H_2O content raw (ppm)	H_2O content bkg (ppm)	H_2O content bkg corr (ppm)	2σ (ppm)
DaG 945									
Ap1a	218	243	211	402	82	78	14	64	2
Ap1b	586	717	679	403	79	68	14	54	2
Ap1c	74	64	40	428	86	100	14	86	3
Ap2a	−25	−53	−84	449	83	81	14	67	2
Ap3a	−25	−46	−55	261	94	243	14	229	7
Ap3b	−17	−44	−79	487	81	74	14	60	2
Ap4	103	98	75	367	87	106	14	92	3
Ap5	110	107	82	367	86	94	14	80	4
Ap6	−366	−425	−441	379	90	145	14	131	7
Ap7b	−79	−106	−119	299	92	172	14	158	8
DaG 844									
Ap1	−87	−107	−109	157	99	1159	14	1145	57
Ap2	−154	−173	−174	185	99	3666	14	3652	181
Ap3	−71	−89	−90	92	99	2444	14	2430	121
Millbillillie									
Ap1a	−49	−76	−80	220	94	275	17	258	9
Ap1b	−101	−126	−127	131	98	860	17	843	31
Ap1c	334	329	326	447	95	330	17	313	12
Ap2	106	85	84	122	98	1080	17	1063	39
Ap3a	239	242	234	299	89	163	17	146	5
Ap3b	95	89	74	373	81	91	17	74	3
Ap4	135	127	118	278	88	147	17	130	5
Stannern									
Section 1 Ap1	23	0	−1	89	99	1860	17	1843	68
Section 2 Ap4a	−8	−39	−40	111	99	1579	23	1556	33
Section 2 Ap4b	17	−13	−14	93	99	1772	23	1749	38
Section 2 Ap2b	47	28	−24	327	62	59	23	36	1
Section 2 Ap2d	−197	−349	−396	416	65	64	23	41	1
Sioux County									
Ap6a	−64	−105	−110	363	90	217	23	194	5
Ap7b	−235	−340	−354	365	78	102	23	79	2
Moore County									
Ap1a	80	94	79	361	57	45	20	25	1
Ap1b	−47	−106	−115	503	69	62	20	42	1
Ap4a	74	83	68	332	58	47	20	27	1
Ap7a	−214	−288	−289	271	84	147	23	124	3
Ap11a	130	129	124	283	78	102	23	79	2

Bkg corr = background corrected.

+679 ± 403‰ (2σ). It is unlikely that terrestrial water would have altered the D/H systematics of some apatite grains and not others located only a few millimeters away; this applies to areas where cracks are pervasive as well as where they are less frequent. Water can diffuse in and out of apatite, and the diffusivity of H in apatite (at $P = 0.1$ MPa) was experimentally determined by Brenan (1993). In that study it was shown that the diffusion of water at temperatures <200 °C is far too slow for exchange between terrestrial waters and apatite. As the maximum temperatures experienced by the two meteorites found in the Sahara are likely to have been significantly below 200 °C, there should have been negligible exchange with terrestrial waters. Besides, we routinely monitor terrestrial contamination during NanoSIMS analysis using real time imaging (see Tartèse et al. [2013] for further details) that allows us to screen any spurious data. Furthermore, there does not appear to be any systematic difference between the H isotopic compositions of meteorite finds and falls, analyzed in this study. Therefore, we are confident that the apatite grains we have analyzed in the meteorite finds have retained their original isotopic H compositions.

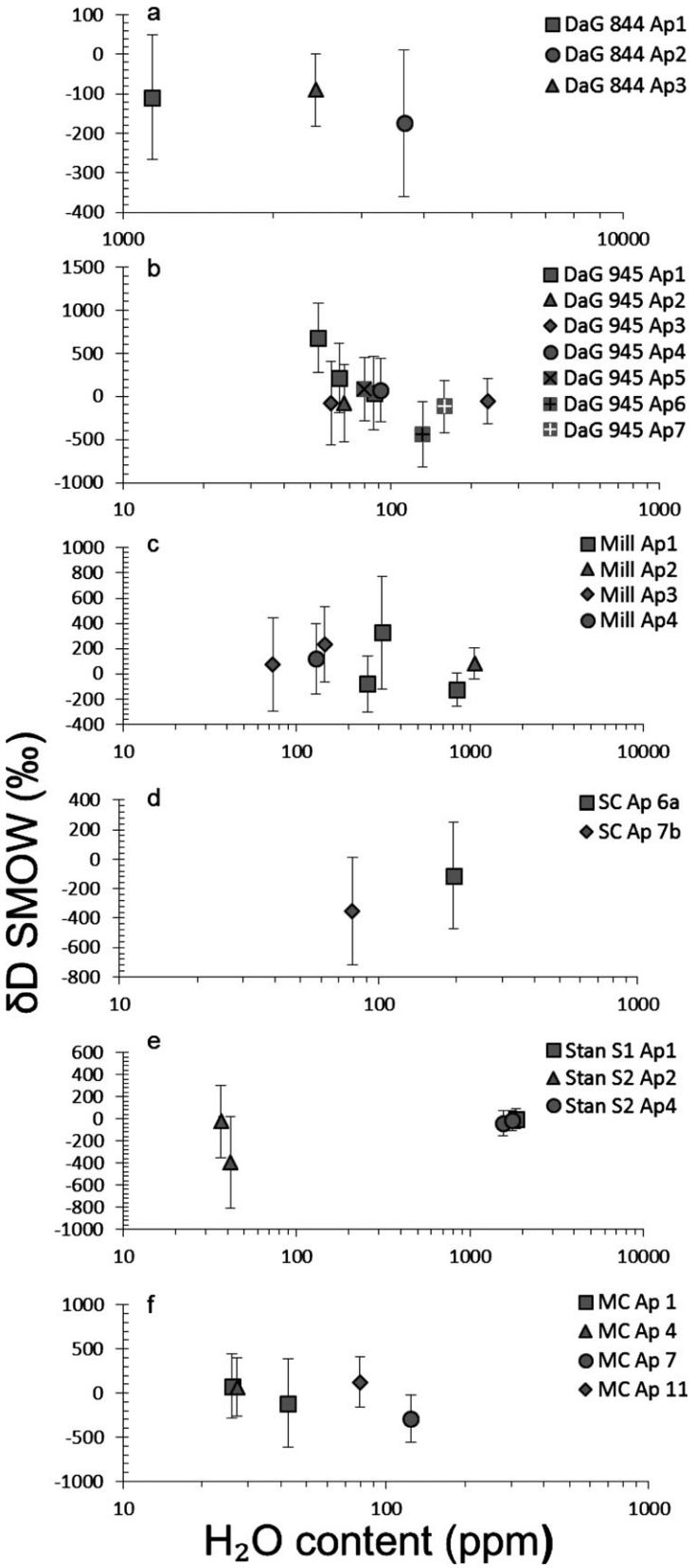

Fig. 2. Plot showing the variations between, and within, apatite grains for the different samples studied.

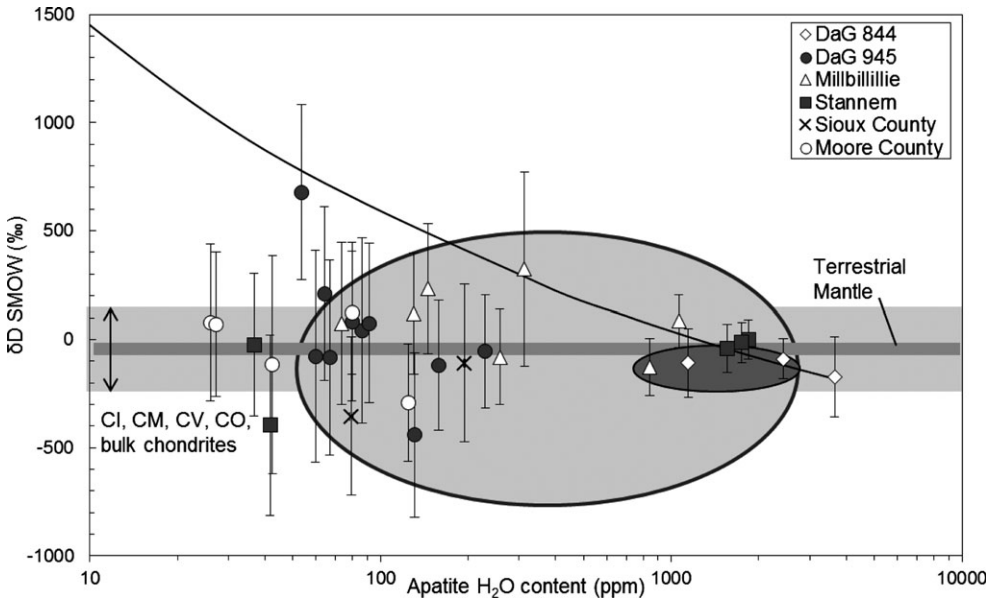

Fig. 3. Plot showing δD values versus H_2O contents of apatite from the studied eucrite meteorites. The thick black line represents the evolution of the δD value of residual water in a magma undergoing H_2 degassing—see text for explanation. Uncertainties are reported at the 2σ level. Gray symbols represent type 4 eucrites, crosses type 5, and white symbols type 6. The light-gray ellipse represents the field for lunar highland samples (Barnes et al. 2014) and the dark gray ellipse highlights the range of previously published δD-H_2O data for apatite in eucrites (Sarafian et al. 2014). The bulk carbonaceous chondrite δD range is derived from Alexander et al. (2012) and the terrestrial range ($-60 \pm 20‰$) taken from Lécuyer et al. (1998). It should be noted that values as low as $-218‰$ have recently been reported for terrestrial lavas (Hallis et al. 2015).

Magmatic Degassing

In the case of lunar picritic glasses and mare basalts, it has been argued that magmatic degassing of volatile species such as H_2 could have caused a strong increase in the D/H ratio of residual water dissolved in the parent melts (Saal et al. 2013; Tartèse and Anand 2013; Tartèse et al. 2013; Füri et al. 2014). This process would have efficiently fractionated the isotopes of hydrogen through the preferential loss of H_2 gas, which enriches the water in the remaining melt in D. Since apatite crystallizes late in the crystallization history of basaltic melts (>90% crystallization, e.g., Sha 2000), it is likely to record elevated D/H signatures and not the undegassed (primitive) magmatic signature, if degassing occurred. To test if magmatic degassing of volatiles such as H_2 could have been an important process during petrogenesis of the studied eucrites, the evolution of the D/H ratio of the water dissolved in the melt during the concomitant degassing of a H_2 gas phase was modeled (Fig. 3). The model obeys the Rayleigh fractionation relationship $R = R_o \times f^{(\alpha-1)}$, where R_o and R are the initial and final D/H ratios of water in the melt, respectively, α is the fractionation factor, and f is the fraction of water remaining in the melt. The most H_2O-rich apatite analysis in this study (DaG 844 Ap2) is considered as the starting point for both H_2O abundance and δD. Figure 3 shows that the $\delta D/H_2O$ systematics of apatite in the studied eucrites do not follow the calculated degassing trend, except for one analysis in DaG 945 (DaG 945 Ap1b), which is characterized by an elevated δD value of $+679 \pm 403‰$. This analysis is from an apatite grain where multiple analyses were undertaken that yielded lower δD values ($+211 \pm 402‰$ and $+40 \pm 428‰$). This particular measurement, while plotting close to the degassing trend, is still within error of the majority of apatite measurements. Excluding this point, all the remaining measured δD values are identical within analytical uncertainty over a range of H_2O contents that vary by more than two orders of magnitude. This suggests that the H isotope signature of eucritic melts was not fractionated by magmatic degassing of H_2. On this basis, the majority of the apatite grains appear to record the magmatic signature of their parental melts. In the case of the lunar basalts, which likely crystallized as lava flows, volatile degassing is believed to have occurred at, or near, the surface of the Moon (Ustunisik et al. 2015). Since the $H_2O/\delta D$ characteristics of apatite grains from eucrites do not hint at any significant degassing effects this could suggest that these eucrites crystallized at depth, which inhibited any significant magmatic degassing.

Petrological, Geochemical, and Metamorphic Trends

No resolvable difference between the H_2O content and δD value of apatite from the Stannern and Main Group/Nuevo Laredo trends is observed within the data presented here. Our results, obtained on DaG 844, yielded apatite δD values and H_2O abundance overlapping with those published by Sarafian et al. (2014) for Stannern (Fig. 3). The apatite δD values of other Main Group eucrites typically show more variation but remain within error of the Stannern trend apatite δD values (Fig. 3). The apatite water content of Main Group eucrites from this study, however, displays a significantly larger range than most of the Stannern apatite values (Fig. 3). This is different from the abundances for other Main Group eucrites reported by Sarafian et al. (2014), which have higher and more restricted water contents (~650–2600 ppm H_2O).

However, apatite in Stannern does show a large variability in H_2O between one grain (see the Criteria for Sample Selection and Petrology of the Studied Samples section) and the other two measured in this study (Fig. 2e). The petrologic context of the two high-H_2O apatite grains is also distinct from that of the low-H_2O grain (See Fig. 1 for high-H_2O apatite grain and Fig. 4 for the low-H_2O apatite). The high-H_2O grains are located in more mesostasis-rich areas, suggestive of late-stage crystallization. The apatite grain containing less H_2O (37 ± 1 and 42 ± 1 ppm H_2O, as opposed to >1500 ppm), on the other hand, appears to have cocrystallized with the silicates surrounding it and, therefore, may have crystallized earlier than the other apatite grains (Fig. 4). This observation is consistent with the evolution of apatite chemistry during fractional crystallization, where earlier crystallized apatite is F-rich and OH-poor and late-crystallizing apatite is more OH-rich (Boyce et al. 2014; McCubbin et al. 2015).

Also, these results do not show any sign of correlation between the $H_2O/\delta D$ characteristics of apatite and the metamorphic grade of the eucrites since apatite from types 4 and 6 eucrites are observed across the entire range of H_2O abundances (Fig. 3). Three of the eucrites in which apatites were analyzed are believed to be polymict eucrites, DaG 844, Millbillillie, and Sioux County (Yamaguchi et al. 1994, 1997). One drawback of studying polymict breccias is that they represent a mixture of different lithologies that may have undergone different thermal and chemical histories. These variations may be reflected in the isotope systematics of minerals belonging to different clasts, which may make interpretation more complex. It has been suggested that many eucrites are monomict, based on the compositional homogeneity of pyroxene. However, Yamaguchi et al. (1994, 1997) have suggested that detailed examination of multiple thin sections of a single monomict breccia sample can reveal small amounts of other lithologies. In the polymict eucrite breccias studied here, apatite grains were selected in areas that display mineralogical relationships (i.e., late-stage mesostasis regions), similar to those in the other basaltic eucrites analyzed in order to minimize the possibility of apatite having an exogenous origin. These apatite grains contain water with a D/H ratio identical to those in the monomict eucrites.

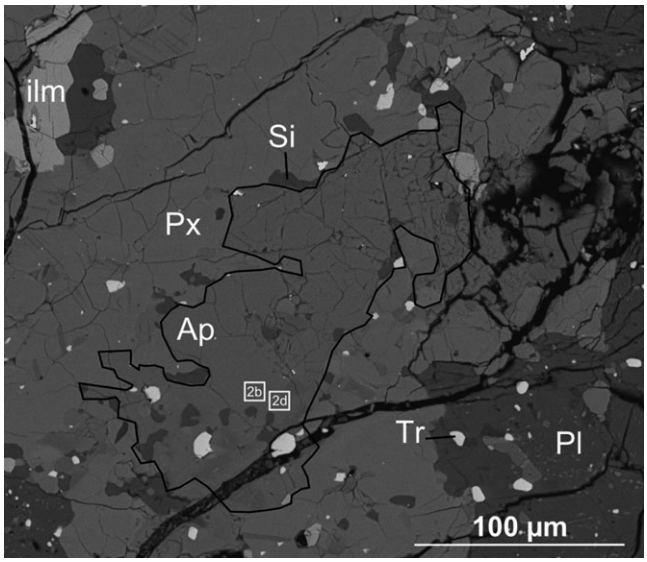

Fig. 4. BSE image of Stannern apatite grain (Section 2 Ap2). Pl = plagioclase, Px = pyroxene, Ap = apatite, Mrl = merrillite, ilm = ilmenite, Tr = troilite, Si = silica phase. Solid white squares represent approximate location of SIMS raster area.

Comparison with Previously Published Data

With the exception of Stannern, the eucrites analyzed here have not been investigated previously for their water content. The results obtained on two of the three Stannern grains (~1500–1800 ppm H_2O and δD around $-20 \pm 100‰$; section 1 Ap1 and section 2 Ap4) analyzed in this study are in close agreement with those reported by Sarafian et al. (2014) (~1500–2600 ppm H_2O and δD around $-75 \pm 36‰$). Apatite in the other eucrites analyzed here, however, show a larger variability in H_2O contents and δD values, with most H_2O contents being a factor of 10 lower than previously published values (Sarafian et al. 2014). Similar to measurements of apatite in lunar plutonic and volcanic rocks, some apatite grains show large intragrain variability in H_2O contents (Tartèse et al. 2013; Barnes et al. 2014). For example, a single apatite grain in Millbillillie (Ap1) showed a range from 257 ± 9 to

842 ± 31 ppm H_2O. Such variations probably reflect crystallization processes, and an increase in the H_2O content from core to rim could reflect increasing H/F and H/Cl ratio in the melt as apatite crystallized (Boyce et al. 2014); however, this was not directly observed as neither F nor Cl was measured in this study.

The weighted average δD value of all apatite grains from this study (−34 ± 67‰; n = 32, 95% confidence) is within error of the upper limit of the weighted average for water in bulk Vesta (−162 ± 127‰) proposed by Sarafian et al. (2014). Combining the data obtained in this study with previously published results gives a weighted average δD value of −151 ± 23‰ (95% confidence level, n = 43).

Possible Origin(s) for H in the Inner Solar System

Since eucrites represent some of the oldest achondrite samples (Misawa et al. 2005; Zhou et al. 2013), determining the origin(s) of water in the HED parent body also provides temporal constraints regarding water delivery in inner solar system bodies, assuming that these bodies accreted largely dry (Boss 1998; Lucey et al. 2006; Albarède 2009). In this case, the ancient age of eucrites (typically 4547 to 4559 Ma) argues in favor of delivery of water very early in the inner solar system from homogeneous sources (Sarafian et al. 2014), but against the gradual increase in D/H ratio with increasing distance from the Sun that has been proposed based on radial temperature gradients and equilibrium factors (Drouart et al. 1999; Mousis et al. 2000).

Early accretion of water to the inner solar system seems at odds with one of the current theories for the Moon's volatile inventory, namely the late delivery of volatiles to the magma ocean (Bottke et al. 2010; Tartèse and Anand 2013; Füri et al. 2014, 2015; Hauri et al. 2015). One possible way to reconcile this apparent conflict is to imagine that the small planetesimals, such as Vesta, acquired their volatiles relatively early from a homogenous reservoir while the Proto-Earth and Proto-Moon accreted largely dry. The large impacts that delivered volatiles to the Earth and the Moon, as suggested by Bottke et al. (2010), could then be comprised of these smaller early planetesimals which have a homogenous D/H ratio. This would account for the seemingly different timings of accretion of volatiles to different parts of the inner solar system while requiring a homogenous D/H reservoir, consistent with the water D/H ratios observed in these different planetary bodies.

Early in the history of the solar system, accreting bodies such as Vesta would have been hot and may have passed through a stage of global melting to produce partial or complete magma oceans (e.g., Snyder et al. 1992; Greenwood et al. 2005; Mandler and Elkins-Tanton 2013). It is plausible during the planetesimals' magma ocean stage that degassing of volatile species could have led to elevated bulk DH ratio (Sharp et al. 2013). However, this would require all inner solar system bodies to degas to a homogenous final D/H ratio, an unlikely scenario given the difference in size between some of these bodies and that degassing was likely to have been more efficient in smaller bodies.

While addition of volatiles to planetesimals after their formation is a possibility, it can also be argued that water is indigenous in inner solar system objects, and that no late addition is necessary. Muralidharan et al. (2008) and King et al. (2010) demonstrated that water can be chemisorbed to fractal forsterite grains even at temperatures previously believed to be too hot for hydrous phases to be thermodynamically stable (Boss 1998). Unless water was fractionated during adsorption on forsterite grains, the D/H ratio of the adsorbed water was likely to be similar to the protosolar δD value of −865‰ (Lellouch et al. 2001). If inner solar system objects accreted water initially characterized by similarly low D/H ratios then a mechanism capable of increasing D/H ratios to the levels observed in inner solar system bodies, about an order of magnitude higher, is required.

Incorporation of materials to explain the increase in D/H ratios from protosolar values is also a valid alternative. Objects formed at greater heliocentric distances, such as comets, seem to be characterized by a much larger range in D/H ratios, ranging from terrestrial-like (e.g., 103P/Hartley 2; Hartogh et al. 2011) to those about three times higher than terrestrial values (e.g., 67P/Churyumov-Gerasimenko; Altwegg et al. 2015). However, these D/H measurements were not made directly on water ice in the comet nucleus, but on the gas emitted during sublimation, which could have different water D/H characteristics (Drake 2005; Drake and Campins 2005). Comets also contain a large amount of organic material, which is typically characterized by elevated D/H ratios (Robert 2006), and therefore, the bulk composition of comets is likely to be more D-rich than cometary water. The addition of a minimum of ~25% cometary material would be required (based on the most elevated D/H ratio measured in 67/P) to elevate solar values to those observed in this study, with much more required if comets with lower D/H ratios were added. Given the uniformity of the bulk D/H ratio of Vesta (inferred from this study) versus the variably elevated D/H ratio of water in most comets, it is unlikely that cometary impacts represent the sole method by which water was delivered to the inner solar system (e.g., Dauphas et al. 2000).

Alternatively, Alexander et al. (2012) demonstrated that the CI chondrites plot on a line connecting solar nebula values for both hydrogen and nitrogen isotopes and bulk Earth, and proposed that a ~10% contribution of solar isotopic composition to compositions similar to those of CI chondrites could explain the D/H ratio of the Earth.

The D/H signatures of water in apatite in eucrites measured in this study (weighted average δD value of $-34 \pm 67‰$) and by Sarafian et al. (2014) (weighted average δD value of $-162 \pm 127‰$) are consistent with D/H values measured in CI, CV, CM, and CO carbonaceous chondrites (Robert 2006; Alexander et al. 2012), terrestrial materials (Lécuyer et al. 1998), and in some lithologies from the Moon (Saal et al. 2013; Tartèse et al. 2013, 2014a; Anand et al. 2014; Barnes et al. 2014) (Fig. 2). The lunar highland samples studied by Barnes et al. (2014) are lunar crustal material and, therefore, potentially provide an indication of the primordial lunar H-isotopic signature, especially because these plutonic samples crystallized deep in the lunar crust around 4.35 Ga ago, likely preventing any significant volatile degassing. Apatite in these rocks have a H_2O content range (~90–1800 ppm H_2O) and δD values similar to those measured in apatite in the eucrites (Fig. 2). Taken together, the striking homogeneity displayed by inner solar system bodies would seem to indicate a common source for water in the inner solar system.

CONCLUSIONS

1. Apatite from eucrites records the indigenous H-isotopic composition of the HED parent body.
2. There is no resolvable difference between the H_2O content and δD values of apatite in the Stannern versus the Main Group-Nuevo Laredo trends.
3. Metamorphism on the HED parent body appears to have had little effect on the H_2O content and δD values of apatite in eucrites.
4. The δD results presented suggest that most eucrites were not affected by volatile degassing.
5. The results from this study provide a fourfold increase in the number of $\delta D/H_2O$ analyses available for apatite in eucrites.
6. The results are consistent with previous study and indicate that water in the HED parent body was characterized by a homogenous reservoir with D/H signatures similar to those of most types of carbonaceous chondrites, the Earth's mantle, and the Moon.

Acknowledgments—This work was funded by a STFC Studentship to TJB and research grant to MA (ST/I001298/1) and a research grant to BLAC, IAF, MA, MMG, RCG, and RT (ST/L000776/1). The following individuals are thanked for providing samples: Alex Bevan (Western Australia Museum, Millbillillie [13357.3]), Francis McCubbin (University of New Mexico, Stannern [UNM1080]), Ludovic Ferrière (Naturhistorisches Museum Wien, Stannern [L4979]), and Linda Welzenbach (Smithsonian Institute, Moore County [USNM 929-2], Sioux County [USNM 896-2]). TJB is grateful to Nicola Potts for general guidance and advice on data interpretation and to Euan Soutter for collecting initial SEM images and X-ray elemental maps of Stannern through an internship, funded by a Paneth Trust for Meteorites award by the Royal Astronomical Society to M. A. We also thank M. Ito, F. M. McCubbin, and the associate editor A. Yamaguchi for their comments.

Editorial Handling—Dr. Akira Yamaguchi

REFERENCES

Albarède F. 2009. Volatile accretion history of the terrestrial planets and dynamic implications. *Nature* 461:1227–1233.

Alexander C. M. O'D., Bowden R., Fogel M. L., Howard K. T., Herd C. D. K., and Nittler L. R. 2012. The provenances of asteroids, and their contributions to the volatile inventories of the terrestrial planets. *Science* 337:721–723.

Altwegg K., Balsiger H., Bar-Nun A., Berthelier J. J., Bieler A., Bochsler P., Briois C., Calmonte U., Combi M., De Keyser J., Eberhardt P., Fiethe B., Fuselier S., Gasc S., Gombosi T. I., Hansen K. C., Hässig M., Jäckel A., Kopp E., Korth A., LeRoy L., Mall U., Marty B., Mousis O., Neefs E., Owen T., Rème H., Rubin M., Sémon T., Tzou C.-Y., Waite H., and Wurz P. 2015. 67P/Churyumov-Gerasimenko, a Jupiter family comet with a high D/H ratio. *Science* 347:1261952-1–1261952-3.

Anand M., Tartèse R., and Barnes J. J. 2014. Understanding the origin and evolution of water in the Moon through lunar sample studies. *Philosophical Transactions of the Royal Society A: Mathematical, Physical and Engineering Sciences* 372:20130254.

Barnes J. J., Franchi I. A., Anand M., Tartèse R., Starkey N. A., Koike M., Sano Y., and Russell S. S. 2013. Accurate and precise measurements of the D/H ratio and hydroxyl content in lunar apatites using NanoSIMS. *Chemical Geology* 337–338:48–55.

Barnes J. J., Tartèse R., Anand M., McCubbin F. M., Franchi I. A., Starkey N. A., and Russell S. S. 2014. The origin of water in the primitive Moon as revealed by the lunar highlands samples. *Earth and Planetary Science Letters* 390:244–252.

Barrat J., Blichert-Toft J., Gillet P., and Keller F. 2000. The differentiation of eucrites: The role of in situ crystallization. *Meteoritics & Planetary Science* 35:1087–1100.

Barrat J., Yamaguchi A., Greenwood R., Bohn M., Cotten J., Benoit M., and Franchi I. 2007. The Stannern trend eucrites: Contamination of main group eucritic magmas by

crustal partial melts. *Geochimica et Cosmochimica Acta* 71:4108–4124.
Binzel R. P. and Xu S. 1993. Chips off of asteroid 4 Vesta: Evidence for the parent body of basaltic achondrite meteorites. *Science* 260:186–191.
Bobe K., Bischoff A., and Stöffler D. 1989. Impact and thermal metamorphism as fundamental processes in the evolution of Stannern, Juvinas, Jonzac, Peramiho, and Millbillillie eucrite parent body (abstract). *Meteoritics* 24:252.
Boss A. P. 1998. Temperatures in protoplanetary disks. *Annual Review of Earth and Planetary Sciences* 26:53–80.
Bottke W. F., Walker R. J., Day J. M. D., Nesvorny D., and Elkins-Tanton L. 2010. Stochastic late accretion to Earth, the Moon, and Mars. *Science* 330:1527–1530.
Boyce J. W., Tomlinson S. M., McCubbin F. M., Greenwood J. P., and Treiman A. H. 2014. The lunar apatite paradox. *Science* 344:400–402.
Brenan J. M. 1993. Kinetics of fluorine, chlorine and hydroxyl exchange in fluorapatite. *Chemical Geology* 110:195–210.
B.V.S.P. 1981. *Basaltic volcanism on the terrestrial planets*. New York: Pergamon Press Inc.
Chambers J. E. and Wetherill G. W. 2001. Planets in the asteroid belt. *Meteoritics & Planetary Science* 36:381–399.
Consolmagno G. J. and Drake M. J. 1977. Composition and evolution of the eucrite parent body: Evidence from rare earth elements. *Geochimica et Cosmochimica Acta* 41:1271–1282.
Dauphas N., Robert F., and Marty B. 2000. The late asteroidal and cometary bombardment of Earth as recorded in water deuterium to protium ratio. *Icarus* 148:508–512.
Delaney J., O'neill C., and Prinz M. 1984. Phosphate minerals in eucrites. Proceedings, 15th Lunar and Planetary Science Conference. pp. 208–209.
Drake M. J. 2005. Origin of water in the terrestrial planets. *Meteoritics & Planetary Science* 40:519–527.
Drake M. J. and Campins H. 2005. Origin of water on the terrestrial planets. *Proceedings of the International Astronomical Union* 1:381–394.
Drouart A., Dubrulle B., Gautier D., and Robert F. 1999. Structure and transport in the solar nebula from constraints on deuterium enrichment and giant planets formation. *Icarus* 140:129–155.
Eugster O., and Michel T. 1995. Common asteroid break-up events of eucrites, diogenites, and howardites and cosmic-ray production rates for noble gases in achondrites. *Geochimica et Cosmochimica Acta* 59:177–199.
Füri E., Deloule E., Gurenko A., and Marty B. 2014. New evidence for chondritic lunar water from combined D/H and noble gas analyses of single Apollo 17 volcanic glasses. *Icarus* 229:109–120.
Füri E., Chaussidon M., and Marty B. 2015. Evidence for an early nitrogen isotopic evolution in the solar nebula from volatile analyses of a CAI from the CV3 chondrite NWA 8616. *Geochimica et Cosmochimica Acta* 153:183–201.
Greenwood R. C., Franchi I. A., Jambon A., and Buchanan P. C. 2005. Widespread magma oceans on asteroidal bodies in the early solar system. *Nature* 435:916–918.
Greenwood J. P., Itoh S., Sakamoto N., Warren P., Taylor L., and Yurimoto H. 2011. Hydrogen isotope ratios in lunar rocks indicate delivery of cometary water to the Moon. *Nature Geoscience* 4:79–82.
Hagemann R., Nief G., and Roth E. 1970. Absolute isotopic scale for deuterium analysis of natural waters. Absolute D/H ratio for SMOW1. *Tellus* 22:712–715.
Hallis L. J., Huss G. R., Nagashima K., Taylor G. J., Halldórsson S. A., Hilton D. R., Mottl M. J., and Meech K. J. 2015. Evidence for primordial water in Earth's deep mantle. *Science* 350:795–797.
Hartogh P., Lis D. C., Bockelée-Morvan D., de Val-Borro M., Biver N., Küppers M., Emprechtinger M., Bergin E. A., Crovisier J., and Rengel M. 2011. Ocean-like water in the Jupiter-family comet 103P/Hartley 2. *Nature* 478:218–220.
Hauri E. H., Weinreich T., Saal A. E., Rutherford M. C., and Van Orman J. A. 2011. High pre-eruptive water contents preserved in lunar melt inclusions. *Science* 333:213–215.
Hauri E. H., Saal A. E., Rutherford M. J., and Van Orman J. A. 2015. Water in the Moon's interior: Truth and consequences. *Earth and Planetary Science Letters* 409:252–264.
Hess H. and Henderson E. 1949. The Moore County meteorite: A further study with comment on its primordial environment. *American Mineralogist* 34:494–507.
Hsu W. and Crozaz G. 1996. Mineral chemistry and the petrogenesis of eucrites: I. Noncumulate eucrites. *Geochimica et Cosmochimica Acta* 60:4571–4591.
Hutchison R. 2004. *Meteorites: A petrologic, chemical and isotopic synthesis*. Cambridge: Cambridge University Press.
Janots E., Gnos E., Hofmann B., Greenwood R., Franchi I., Bermingham K., and Netwing V. 2012. Jiddat al Harasis 556: A howardite impact melt breccia with an H chondrite component. *Meteoritics & Planetary Science* 47:1558–1574.
King H., Stimpfl M., Deymier P., Drake M., Catlow C., Putnis A., and de Leeuw N. 2010. Computer simulations of water interactions with low-coordinated forsterite surface sites: Implications for the origin of water in the inner solar system. *Earth and Planetary Science Letters* 300:11–18.
Lécuyer C., Gillet P., and Robert F. 1998. The hydrogen isotope composition of seawater and the global water cycle. *Chemical Geology* 145:249–261.
Lellouch E., Bézard B., Fouchet T., Feuchtgruber H., Encrenaz T., and de Graauw T. 2001. The deuterium abundance in Jupiter and Saturn from ISO-SWS observations. *Astronomy & Astrophysics* 370:610–622.
Lucey P., Korotev R. L., Gillis J. J., Taylor L. A., Lawrence D., Campbell B. A., Elphic R., Feldman B., Hood L. L., and Hunten D. 2006. Understanding the lunar surface and space-moon interactions. *Reviews in Mineralogy and Geochemistry* 60:83–219.
Mandler B. E. and Elkins-Tanton L. T. 2013. The origin of eucrites, diogenites, and olivine diogenites: Magma ocean crystallization and shallow magma chamber processes on Vesta. *Meteoritics & Planetary Science* 48:2333–2349.
Mayne R., McSween H., McCoy T., and Gale A. 2009. Petrology of the unbrecciated eucrites. *Geochimica et Cosmochimica Acta* 73:794–819.
McCord T. B., Adams J. B., and Johnson T. V. 1970. Asteroid Vesta: Spectral reflectivity and compositional implications. *Science* 168:1445–1447.
McCubbin F. M., Jolliff B. L., Nekvasil H., Carpenter P. K., Zeigler R. A., Steele A., Elardo S. M., and Lindsley D. H. 2011. Fluorine and chlorine abundances in lunar apatite: Implications for heterogeneous distributions of magmatic volatiles in the lunar interior. *Geochimica et Cosmochimica Acta* 75:5073–5093.

McCubbin F. M., Hauri E. H., Elardo S. M., Vander Kaaden K. E., Wang J., and Shearer C. K. 2012. Hydrous melting of the Martian mantle produced both depleted and enriched shergottites. *Geology* 40:683–686.

McCubbin F. M., Shearer C. K., Burger P. V., Hauri E. H., Wang J., Elardo S. M., and Papike J. J. 2014. Volatile abundances of coexisting merrillite and apatite in the Martian meteorite Shergotty: Implications for merrillite in hydrous magmas. *American Mineralogist* 99:1347–1354.

McCubbin F. M., Vander Kaaden K. E., Tartèse R., Boyce J. W., Mikhail S., Whitson E. S., Bell A. S., Anand M., Franchi I. A., Wang J., and Hauri E. H. 2015. Experimental investigation of F, Cl, and OH partitioning between apatite and Fe-rich basaltic melt at 1.0–1.2 GPa and 950–1000 °C. *American Mineralogist* 100:1790–1802.

Merlivat L., Lelu M., Nief G., and Roth E. 1976. Spallation deuterium in rock 70215. Proceedings, 7th Lunar and Planetary Science Conference. pp. 649–658.

Misawa K., Yamaguchi A., and Kaiden H. 2005. U-Pb and 207Pb-206Pb ages of zircons from basaltic eucrites: Implications for early basaltic volcanism on the eucrite parent body. *Geochimica et Cosmochimica Acta* 69:5847–5861.

Mittlefehldt D. W. and Lindstrom M. M. 2003. Geochemistry of eucrites: Genesis of basaltic eucrites, and Hf and Ta as petrogenetic indicators for altered Antarctic eucrites. *Geochimica et Cosmochimica Acta* 67:1911–1934.

Miura Y., Nagao K., Sugiura N., Fujitani T., and Warren P. 1998. Noble gases, 81Kr-Kr exposure ages and 244Pu-Xe ages of six eucrites, Béréba, Binda, Camel Donga, Juvinas, Millbillillie, and Stannern. *Geochimica et Cosmochimica Acta* 62:2369–2387.

Mousis O., Gautier D., Bockelée-Morvan D., Robert F., Dubrulle B., and Drouart A. 2000. Constraints on the formation of comets from D/H ratios measured in H2O and HCN. *Icarus* 148:513–525.

Muralidharan K., Deymier P., Stimpfl M., de Leeuw N. H., and Drake M. J. 2008. Origin of water in the inner solar system: A kinetic Monte Carlo study of water adsorption on forsterite. *Icarus* 198:400–407.

O'Brien D. P., Walsh K. J., Morbidelli A., Raymond S. N., and Mandell A. M. 2014. Water delivery and giant impacts in the "Grand Tack" scenario. *Icarus* 239:74–84.

Patiño Douce A. E. and Roden M. 2006. Apatite as a probe of halogen and water fugacities in the terrestrial planets. *Geochimica et Cosmochimica Acta* 70:3173–3196.

Patiño Douce A. E., Roden M. F., Chaumba J., Fleisher C., and Yogodzinski G. 2011. Compositional variability of terrestrial mantle apatites, thermodynamic modeling of apatite volatile contents, and the halogen and water budgets of planetary mantles. *Chemical Geology* 288:14–31.

Robert F. 2006 Solar system deuterium/hydrogen ratio. In *Meteorites and the early solar system*, edited by Lauretta D. S, and McSween H. Y. Jr. Tucson, Arizona: The University of Arizona Press. pp. 341–351.

Saal A. E., Hauri E. H., Cascio M. L., Van Orman J. A., Rutherford M. C., and Cooper R. F. 2008. Volatile content of lunar volcanic glasses and the presence of water in the Moon's interior. *Nature* 454:192–195.

Saal A. E., Hauri E. H., Van Orman J. A., and Rutherford M. J. 2013. Hydrogen isotopes in lunar volcanic glasses and melt inclusions reveal a carbonaceous chondrite heritage. *Science* 340:1317–1320.

Saighi O., Michelot J. L., and Filly A. 2001. Isotopic characteristic of meteoric water and groundwater in Ahaggar massif (central Sahara). *International Atomic Energy Agency TECDOC* 1207:7–25.

Sarafian A. R., Roden M. F., and Patiño-Douce A. E. 2013. The volatile content of Vesta: Clues from apatite in eucrites. *Meteoritics & Planetary Science* 48:2135–2154.

Sarafian A. R., Nielsen S. G., Marschall H. R., McCubbin F. M., and Monteleone B. D. 2014. Early accretion of water in the inner solar system from a carbonaceous chondrite–like source. *Science* 346:623–626.

Sha L.-K. 2000. Whitlockite solubility in silicate melts: Some insights into lunar and planetary evolution. *Geochimica et Cosmochimica Acta* 64:3217–3236.

Sharp Z. D., McCubbin F. M., and Shearer C. K. 2013. A hydrogen-based oxidation mechanism relevant to planetary formation. *Earth and Planetary Science Letters* 380:88–97.

Snyder G. A., Taylor L. A., and Neal C. R. 1992. A chemical model for generating the sources of mare basalts: Combined equilibrium and fractional crystallization of the lunar magmasphere. *Geochimica et Cosmochimica Acta* 56:3809–3823.

Stolper E. 1977. Experimental petrology of eucritic meteorites. *Geochimica et Cosmochimica Acta* 41:587–611.

Takeda H. and Graham A. 1991. Degree of equilibration of eucritic pyroxenes and thermal metamorphism of the earliest planetary crust. *Meteoritics* 26:129–134.

Tartèse R. and Anand M. 2013. Late delivery of chondritic hydrogen into the lunar mantle: Insights from mare basalts. *Earth and Planetary Science Letters* 361:480–486.

Tartèse R., Anand M., Barnes J. J., Starkey N. A., Franchi I. A., and Sano Y. 2013. The abundance, distribution, and isotopic composition of Hydrogen in the Moon as revealed by basaltic lunar samples: Implications for the volatile inventory of the Moon. *Geochimica et Cosmochimica Acta* 122:58–74.

Tartèse R., Anand M., Joy K. H., and Franchi I. A. 2014a. H and Cl isotope systematics of apatite in brecciated lunar meteorites Northwest Africa 4472, Northwest Africa 773, Sayh al Uhaymir 169, and Kalahari 009. *Meteoritics & Planetary Science* 49:2266–2289.

Tartèse R., Anand M., McCubbin F. M., Elardo S. M., Shearer C. K., and Franchi I. A. 2014b. Apatites in lunar KREEP basalts: The missing link to understanding the H isotope systematics of the Moon. *Geology* 42:363–366.

Ustunisik G., Nekvasil H., Lindsley D. H., and McCubbin F. M. 2015. Degassing pathways of Cl-, F-, H-, and S-bearing magmas near the lunar surface: Implications for the composition and Cl isotopic values of lunar apatite. *American Mineralogist* 100:1717–1727.

Warren P. H. and Jerde E. A. 1987. Composition and origin of Nuevo Laredo trend eucrites. *Geochimica et Cosmochimica Acta* 51:713–725.

Yamaguchi A., Takeda H., Bogard D. D., and Garrison D. 1994. Textural variations and impact history of the Millbillillie eucrite. *Meteoritics* 29:237–245.

Yamaguchi A., Taylor G. J., and Keil K. 1996. Global crustal metamorphism of the eucrite parent body. *Icarus* 124:97–112.

Yamaguchi A., Taylor G., and Keil K. 1997. Not all eucrites are monomict breccias (abstract #1601). 28th Lunar and Planetary Science Conference. CD-ROM.

Yamaguchi A., Barrat J. A., Greenwood R. C., Shirai N., Okamoto C., Setoyanagi T., Ebihara M., Franchi I. A., and Bohn M. 2009. Crustal partial melting on Vesta: Evidence from highly metamorphosed eucrites. *Geochimica et Cosmochimica Acta* 73:7162–7182.

Zhou Q., Yin Q.-Z., Young E. D., Li X.-H., Wu F.-Y., Li Q.-L., Liu Y., and Tang G.-Q. 2013. SIMS Pb–Pb and U-Pb age determination of eucrite zircons at <5 μm scale and the first 50 Ma of the thermal history of Vesta. *Geochimica et Cosmochimica Acta* 110:152–175.